Structural Characterization of Layered $Li_xNi_{0.5}Mn_{0.5}O_2$ ($0 < x \leq 2$) Oxide Electrodes for Li Batteries

Christopher S. Johnson,*,† Jeom-Soo Kim,† A. Jeremy Kropf,† Arthur J. Kahaian,† John T. Vaughey,† Linda M. L. Fransson,‡ Kristina Edström,‡ and Michael M. Thackeray†

Electrochemical Technology and Basic Sciences Program, Chemical Technology Division, Argonne National Laboratory, Argonne, Illinois 60439, and Department of Materials Chemistry, Ångstrom Laboratory, Uppsala University, Sweden

Received October 11, 2002. Revised Manuscript Received January 7, 2003

X-ray diffraction and X-ray absorption spectroscopy experiments were used to study chemical and electrochemical Li insertion and extraction reactions of $LiNi_{0.5}Mn_{0.5}O_2$. These results, along with galvanostatic cycling data, suggest that $LiNi_{0.5}Mn_{0.5}O_2$ layered electrodes in lithium batteries operate predominantly off two-electron redox couples, Ni^{4+}/Ni^{2+}, between approximately 4.5 and 1.25 V and Mn^{4+}/Mn^{2+} between 1.25 and 1.0 V versus metallic Li, respectively. The retention of a stable layered framework structure and the apparent absence of Jahn−Teller ions Ni^{3+} and Mn^{3+} in the high- or low-voltage region is believed to be responsible for the excellent structural and electrochemical stability of these electrodes. The $LiNi_{0.5}Mn_{0.5}O_2$ layered oxide reversibly reacts chemically or electrochemically with Li to form an air-sensitive, dilithium compound, $Li_2Ni_{0.5}Mn_{0.5}O_2$, with a hexagonal structure analogous to Li_2MnO_2. The cycling behavior of $Li/LiNi_{0.5}Mn_{0.5}O_2$ cells over a large voltage window (4.6−1.0 V) and with very slow rates shows that rechargeable capacities >500 mA·h/g can be obtained.

1. Introduction

Layered transition metal oxides ($LiMO_2$; M = transition metal ion) such as lithium cobalt oxide ($LiCoO_2$), lithium nickel oxide ($LiNiO_2$), or lithium nickel−cobalt oxides ($LiNi_{1-z}Co_zO_2$) have been widely studied as cathodes for Li-ion batteries.[1−3] Ideally, these materials have a rock-salt structure with space group symmetry $R\bar{3}m$. When used in a battery, the charge is stored and released via redox changes at the metal center. In phase-pure systems, and in the simplest of cases, the metal(s) undergoes a reversible one-electron process shuttling back and forth from trivalent to tetravalent oxidation states.[4] Earlier synthesis and electrochemical studies had shown that it is possible to replace some of the trivalent nickel in $LiNiO_2$ with Mn to give a $Li_xNi_{1-y}Mn_yO_2$ ($0 \leq y \leq 0.5$, $0.9 \leq x < 1.2$) solid solution.[5,6] In these studies, when the value of y was increased from 0.1 to 0.5, then the formation of more Mn^{4+} was speculated and overall charge neutrality was satisfied by additional Li^+ with Ni^{3+}. Recently, half of the nickel was substituted by manganese in the synthesis of layered $LiNi_{0.5}Mn_{0.5}O_2$ from a metal double-hydroxide route.[7] This material demonstrates good electrochemical stability and reversibility and delivers about 150 mA·h/g after 30 cycles between 2.5 and 4.3 V.[7,8] In this 50:50 molar mixture, the M cations have nominally an average oxidation state of +3. However, from the electrochemistry and cycling results,[9,10] and first principles calculations,[11] the charge distribution for $LiNi_{0.5}Mn_{0.5}O_2$ has been predicted to be Ni^{2+} and Mn^{4+}.

Layered $LiNi_{0.5}Mn_{0.5}O_2$ was also previously synthesized via a high-temperature reaction of lithium hydroxide with a prepared metal oxyhydroxide precursor, $Li_xNi_{0.5}Mn_{0.5}O(OH)$, where $x = 0.24$.[12] The $Li_xNi_{0.5}Mn_{0.5}O(OH)$ was produced by a different method using metal nitrates oxidized and coprecipitated from a Br_2/LiOH (LiOBr) aqueous solution. Interestingly, this product was identified to be trivalent Ni^{3+} and Mn^{3+} from combined ex situ magnetic susceptibility and X-ray photoelectron spectroscopy (XPS) data. The capacity of this $LiNi_{0.5}Mn_{0.5}O_2$ electrode declines from an initial 160 to 80 mA·h/g at the 50th cycle from 2.5 to 4.3 V.

In this paper, detailed results of electrochemical and structural evaluations of a layered $LiNi_{0.5}Mn_{0.5}O_2$ starting material and its delithiated and lithiated products

* Corresponding author. E-mail: johnsoncs@cmt.anl.gov.
† Argonne National Laboratory.
‡ Uppsala University.

(1) Mitzushima, K.; Jones, P. C.; Wiseman, P. J.; Goodenough, J. B. *Mater. Res. Bull.* **1980**, *15*, 783.
(2) Alcantara, R.; Lavela, P.; Tirado, J. L.; Zhecheva, E.; Stoyanova, R. *J. Solid State Electrochem.* **1999**, *3*, 121.
(3) Saadoune, I.; Delmas, C. *J. Solid State Chem.* **1998**, *136*, 8.
(4) Ohzuku, T.; *Lithium Batteries. New Materials, Developments and Perspectives*; Pistoia, G., Ed.; Elsevier: Amsterdam, 1994.
(5) Rossen, R.; Jones, C. D. W.; Dahn, J. R. *Solid State Ionics* **1992**, *57*, 311.
(6) Yoshio, M.; Todorov, Y.; Yamato, K.; Noguchi, H.; Itoh, J.; Okada, M.; Mouri, T. *J. Power Sources* **1998**, *74*, 46.
(7) Ohzuku, T.; Makimura, Y. *Chem. Lett.* **2001**, 744.
(8) Lu, Z.; MacNeil, D. D.; Dahn, J. R. *Electrochem. Solid State Lett.* **2001**, *4*, A191.
(9) Kim, J.-S.; Johnson, C. S.; Thackeray, M. M. *Electrochem. Commun.* **2002**, *4*, 205.
(10) Lu, J.; Beaulieu, L. Y.; Donaberger, R. A.; Thomas, C. L.; Dahn, J. R. *J. Electrochem. Soc.* **2002**, *149*, A778.
(11) Reed, J.; Ceder, G. *Electrochem. Solid State Lett.* **2002**, *5*, A145.
(12) Spahr, M. E.; Novak, P.; Schnyder, B.; Haas, O.; Nesper, R. *J. Electrochem. Soc.* **1998**, *145*, 1113.

10.1021/cm0204728 CCC: $25.00
Published on Web 05/20/2003

are reported. Of particular significance was our earlier discovery that Li/$LiNi_{0.5}Mn_{0.5}O_2$ cells could be cycled over a large voltage window between 4.6 and 1.0 V with surprisingly good reversibility, leading to capacities in excess of 300 mA·h/g at moderate rates.[13,14] To address the underlying factors associated with the large capacities observed, additional synthesis, X-ray diffraction (XRD), and X-ray absorption spectroscopy (XAS) on the $LiNi_{0.5}Mn_{0.5}O_2$ layered oxide electrode were conducted. Furthermore, we have obtained the crystallographic data for the dilithium, layered compound, $Li_2Ni_{0.5}Mn_{0.5}O_2$ ($x \sim 2$). The retention of a layered $Ni_{0.5}Mn_{0.5}O_2$ oxide framework and the lack of formation of the Jahn−Teller ions, Mn^{3+} or Ni^{3+}, throughout the electrochemical or chemical reaction sequence are believed to be major factors responsible for the excellent reversibility of this system over such a wide voltage window. The objective of this study is to directly determine what metal oxidation states and structural phases are present and to determine the charge compensation mechanism that occurs during cycling of $Li_xNi_{0.5}Mn_{0.5}O_2$ electrodes.

2. Experimental Section

The compound $LiNi_{0.5}Mn_{0.5}O_2$ was prepared in air from a 900−950 °C high-temperature reaction of lithium hydroxide monohydrate (Aldrich 98+%) and a dihydroxide precursor $Ni_{0.5}Mn_{0.5}(OH)_2$ as described previously.[9] The as-prepared $LiNi_{0.5}Mn_{0.5}O_2$ material was lithiated chemically with a 50% mole excess of 0.1 M lithium naphthalide solution that had been freshly prepared from naphthalene (Aldrich, 98%) and metallic lithium (FMC Corp., Lithium Div., 99+%) in tetrahydrofuran (THF; Aldrich 99+%) solvent at room temperature for 24 h. The product was filtered and washed in diethyl ether (Aldrich, 99+%) inside a nitrogen glovebox (<5 ppm H_2O), then subsequently transferred, and stored in a recirculating/purifying He atmosphere (Vacuum Atmospheres, DLX Series; <5 ppm O_2) glovebox prior to X-ray diffraction analysis. Inductively coupled plasma-atomic emission spectrometry (ICP-AES) using an Atomscan Advantage (Thermo Jarrell Ash) spectrometer was used to measure the Li:Ni:Mn metal mole ratios in the starting material and lithiated product. The powder X-ray diffraction data of the starting material and lithiated product were collected on a Siemens D5000 powder diffractometer with Cu Kα radiation. The lithiated powder was loaded onto the sample holder and protected from moisture and air (oxygen, CO_2) with a beryllium foil cover. Samples were scanned between 10° and 80° 2θ at a scan rate of 0.6° 2θ/min. A linear least-squares fit and Rietveld refinements (GSAS program[15]) of the diffraction peaks were used to calculate unit cell parameters.

Electrodes were fabricated from an intimate mixture of the $LiNi_{0.5}Mn_{0.5}O_2$ powder that comprised 85 wt % of the total electrode with 8% poly(vinylidene difluoride) (PVDF) polymer binder (Kynar, Elf-Atochem) and 7% acetylene black (Cabot) in 1-methyl-2-pyrrolidinone (Aldrich, 99+%). The electrode mixture was dried at 75 °C for 10 h, thoroughly ground, pressed into pellets on a stainless steel mesh (Exmet Corp.), and dried again under vacuum at 70 °C for 12 h. The electrodes were evaluated at room temperature in coin-type cells (size 2032, Hohsen) with a lithium foil counter electrode (FMC Corp., Lithium Div.), glass-fiber separator (Gelman Sciences), and an electrolyte consisting of a 1 M $LiPF_6$ solution in ethylene carbonate:diethyl carbonate (1:1) (Merck). Cells were constructed inside a He glovebox (<5 ppm, H_2O and O_2) and cycled on a Maccor Series 2000 tester in galvanostatic mode.

A "coffee-bag" Li/electrolyte/$LiNi_{0.5}Mn_{0.5}O_2$ cell, similar to that described in ref 16, was used for the in situ XRD experiments. Experiments were conducted at Uppsala University, Sweden. Electrodes were fabricated from an intimate mixture of the $LiNi_{0.5}Mn_{0.5}O_2$ powder that comprised 84 wt % of the total electrode with 8% PVDF polymer binder (Kynar) and 4% acetylene black (Cabot), 4% synthetic graphite (Timcal) slurried in 1-methyl-2-pyrrolidinone (NMP). An electrode laminate was cast onto an Al current collector foil using a doctor-blade. The laminate was subsequently dried first at 75 °C for 10 h and then under vacuum at 70 °C for 12 h. The electrolyte used was 1 M $LiPF_6$ in EC:DEC (2:1). The "coffee-bag" cell was cycled at a slow constant current (0.06 mA/cm^2) to a preset voltage and then allowed to relax for at least 3 h for cell equilibration. X-ray diffraction (XRD) patterns were collected after the voltage had stabilized. The position of the cell and the measurement spot remained the same throughout the experiment. Data were collected in a transmission mode with a position-sensitive detector.

The XAS measurements, which included both X-ray absorption near-edge spectroscopy (XANES) and extended X-ray absorption fine structure (EXAFS) techniques, were performed on the insertion device (undulator A) beamline of the Materials Research Collaborative Access Team (MRCAT) at the Advanced Photon Source (APS), Argonne National Laboratory. The details of the equipment and setup are described in detail in ref 17. Samples were prepared in the He glovebox by thoroughly mixing (Wig-L-Bug mixer, REFLEX Analytical Corp.) the $LiNi_{0.5}Mn_{0.5}O_2$ or $Li_2Ni_{0.5}Mn_{0.5}O_2$ powder with boron nitride (BN) as a diluent in a 1:2.5 (sample:BN) weight ratio. In addition, a XANES and EXAFS spectrum of the cathode material laminate taken from a fully charged coin cell (2032 size; single charge to 4.6 V) was also measured. The electrode had been equilibrated in its charged state by holding the voltage of the cell at 4.6 V for 15 h, at which point the current was <20 μA. The cell was subsequently opened in the He glovebox and the laminate recovered and dried under vacuum at room temperature prior to measurement. The standards for the Mn K-edge were Li_2MnO_3 (Mn^{4+}, Strem Chemicals, 99%), Mn_2O_3 (Mn^{3+}, Aldrich, 99%), and MnO (Mn^{2+}, Alfa-Aesar, 99%). The standards for the Ni K-edge were $LiNiO_2$ (Ni^{3+}, synthesized in-house, verified by XRD) and NiO (Ni^{2+}, dark green, Alfa-Aesar, 99%). The standard powders were also mixed with BN diluent in an appropriate ratio. Nickel and manganese metal foils were used to calibrate the energy at each edge. The Ni edge was calibrated such that the first inflection in the Ni metal edge was set to 8333 eV, while the first inflection for the Mn edge was set to 6538 eV. All the samples were loaded on a multiple sample mount and individually covered with Kapton tape to minimize exposure to moisture and air. The XANES and EXAFS spectra were collected first for samples that were known to be moisture-sensitive, particularly the chemically lithiated sample.

3. Results and Discussion

3.1. Synthesis, Composition, and Structure of $Li_xNi_{0.5}Mn_{0.5}O_2$ Layered Oxides. The exact metal ratio composition of the starting material $LiNi_{0.5}Mn_{0.5}O_2$ as-prepared was determined by ICP-AES to be $Li_{0.906}Ni_{0.506}Mn_{0.494}O_2$. Since the product was Li-deficient, the oxygen content was fixed at stoichiometric ($2O^{2-}$) because layered transition metal oxides such as $LiCoO_2$ that are synthesized in air or pure oxygen are not normally oxygen-deficient.[18] On the basis of this com-

(13) Johnson, C. S.; Kim, J.-S.; Kropf, A. J.; Vaughey, J. T.; Thackeray, M. M. *11-IMLB Book of Abstracts*, Abstract No. 119, The Electrochemical Society, June 23−29, 2002.

(14) Johnson, C. S.; Kahaian, A. J.; Kim, J.-S.; Kropf, A. J.; Vaughey, J. T.; Thackeray, M. M. *Electrochem. Commun.* **2002**, *4*, 492.

(15) Larson, A. C.; Von Dreele, R. B. *GSAS−General Structure Analysis System*; Report No. LA-UR-86-748; Los Alamos National Laboratory: Los Alamos, NM, 1990.

(16) Fransson, L. M. L.; Vaughey, J. T.; Benedek, R.; Edstrom, K.; Thomas, J. O.; Thackeray, M. M. *Electrochem. Commun.* **2001**, *3*, 317.

(17) Johnson, C. S.; Kropf, A. J. *Electrochim. Acta* **2002**, *47*, 3187.

(18) Levasseur, S.; Menetrier, M.; Suard, E.; Delmas, C. *Solid State Ionics* **2000**, *128*, 11.

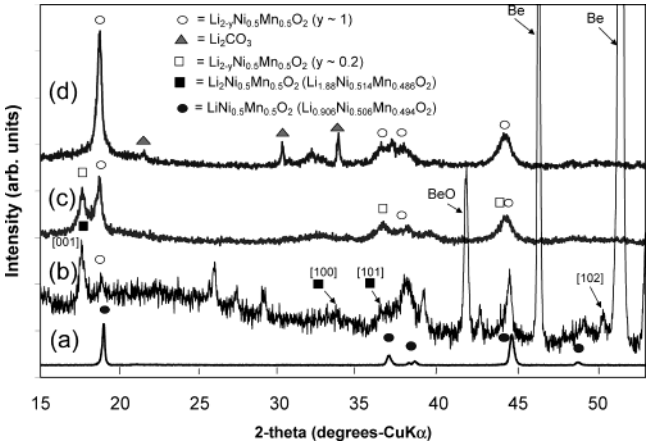

Figure 1. XRD patterns of layered $Li_xNi_{0.5}Mn_{0.5}O_2$ oxides: from bottom to top, (a) as-prepared starting material $LiNi_{0.5}Mn_{0.5}O_2$ ($Li_{0.906}Ni_{0.506}Mn_{0.494}O_2$) (scale factor: 0.15); (b) chemically lithiated $Li_2Ni_{0.5}Mn_{0.5}O_2$ ($Li_{1.88}Ni_{0.514}Mn_{0.486}O_2$) under Be foil cover; (c) sample in b, after 2 h of air exposure; and (d) sample in b after 10 h of air exposure.

position, it appears that some lithium is lost from the sample during the high-temperature reaction, probably in the form of lithia (Li_2O). The Ni/Mn ratio (1.03/1.00) deviated very slightly from the expected ratio (1/1). If it is assumed that the Mn is fully tetravalent 4^+ in this composition, then the Ni is slightly oxidized to 2.2^+ in this material.

The powder X-ray diffraction pattern (XRD) of $LiNi_{0.5}Mn_{0.5}O_2$ ($Li_{0.906}Ni_{0.506}Mn_{0.494}O_2$) is shown in Figure 1 (label a). The structure of the ideal layered compound $LiNi_{0.5}Mn_{0.5}O_2$ with the Ni and Mn randomly distributed over the transition-metal site has been assigned to the α-$NaFeO_2$-structure type (rhombohedral space group $R\bar{3}m$) because it is so closely related to the structure of $LiNiO_2$.[19] The lattice parameters of the $LiNi_{0.5}Mn_{0.5}O_2$ material were calculated from the XRD by Rietveld profile refinement. The unit cell was a = 2.881(1) Å and c = 14.278(2) Å with an overall cell volume of 102.61 Å^3. These parameters are consistent with literature values.[7,8] The lithium atoms fill octahedral sites of one layer, while the nickel and manganese atoms fill the octahedral positions of adjacent layers.

Lithium naphthalide ($Li[C_{10}H_8]$) was used to chemically lithiate $LiNi_{0.5}Mn_{0.5}O_2$. The reduced anion naphthalide $[C_{10}H_8]^-$ was made by reacting naphthalene with lithium metal under argon. $[C_{10}H_8]^-$ in THF is a strong reducing agent with a reduction potential of approximately 0.8 V vs Li metal.[20] Within 5 min of forming the $[C_{10}H_8]^-$, the $LiNi_{0.5}Mn_{0.5}O_2$ powder was added to the solution. A slight color change was observed on treatment of the $LiNi_{0.5}Mn_{0.5}O_2$ powder from jet-black to a dark purple upon lithiation at room temperature. Other chemical lithiation experiments employing either *n*-BuLi in hexanes (at room temperature or under reflux) or Li metal dissolved in liquid ammonia (NH_3) proved to be too harsh for the $LiNi_{0.5}Mn_{0.5}O_2$ oxide and caused severe degradation of the layered structure.

The XRD pattern of the lithiated product synthesized from $Li_{0.906}Ni_{0.506}Mn_{0.494}O_2$ is shown in Figure 1 (label b). The pattern was indexed to space group $P\bar{3}m1$; the

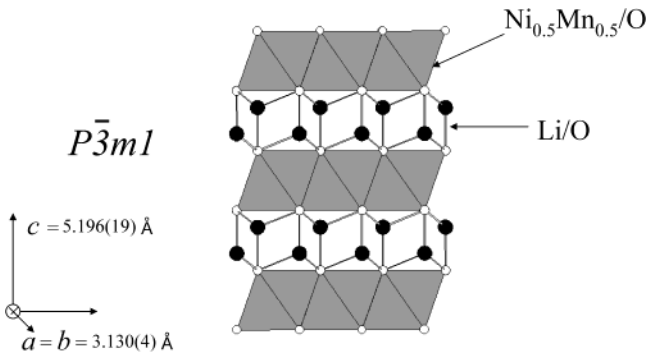

Figure 2. Hexagonally close-packed structure of $Li_2Mn_{0.5}Ni_{0.5}O_2$ showing the Mn^{2+} and Ni^{2+} ions in the octahedral sites of one layer and the Li^+ ions in the tetrahedral sites of adjacent layers.

strongest reflections have been marked in the figure. Lithium, nickel, and manganese metal analysis revealed a stoichiometry of $Li_{1.88}Ni_{0.514}Mn_{0.486}O_2$ for the lithiated product. The Ni/Mn ratio is calculated as 1.06/1.00 and the Li/Ni + Mn mole sum ratio is 1.88/1.00. This value is very near the target mole ratio of 2/1 for $Li_2Ni_{0.5}Mn_{0.5}O_2$. For simplicity, the ideal compositions of $LiNi_{0.5}Mn_{0.5}O_2$ and $Li_2Ni_{0.5}Mn_{0.5}O_2$ will be primarily used in the remaining text of the paper.

In the $Li_2Ni_{0.5}Mn_{0.5}O_2$ structure, which has hexagonal symmetry, the oxygen ions are arranged in a hexagonally close-packed (hcp) array; the M ions are located in all the octahedral sites of one layer and the Li ions are located in all the tetrahedral sites of adjacent layers.[21] The [001] (or [010]) projection of the structure is shown in Figure 2. In this structure, which has also been observed for Li_2NiO_2[22] and Li_2MnO_2,[23] the Li^+−Li^+ distance in edge-shared tetrahedra is short (~2.2 Å) compared with the typical Li^+−Li^+ distances in edge-shared octahedra in related layered structures such as Li_2MnO_3 (2.70−2.92 Å) or $LiCoO_2$ (2.81 Å).

A magnified view of the $Li_2Ni_{0.5}Mn_{0.5}O_2$ XRD spectra between 15 and 22° 2θ is provided in Figure 3. Note that the peak in Figure 3a (or Figure 1b) at approximately 18.8° 2θ is associated with a small amount (<10%) of $LiNi_{0.5}Mn_{0.5}O_2$. The presence of some apparent unreacted material in the sample is evident in the XRD pattern (marked by ↓ in Figure 3a). This result may be attributed either to an incomplete reaction or to the instability of the highly lithiated structure and its tendency to extrude lithium at the particle surface when exposed to air, as discussed below.

With use of a Rietveld profile refinement fit (R_p = 4%), the lattice parameters of $Li_2Ni_{0.5}Mn_{0.5}O_2$ are a = 3.130(4) Å and c = 5.196(19) Å; the corresponding volume of the unit cell, 44.09 Å^3, represents an increase of ~22% in the crystallographic volume of the layered structure on lithiating $LiNi_{0.5}Mn_{0.5}O_2$. The $Li_2Ni_{0.5}Mn_{0.5}O_2$ product is air- and/or moisture-sensitive and is easily oxidized. After 2 h of exposure to air, the sample delithiates to form a two-phase product that consists of $Li_{2-y}Ni_{0.5}Mn_{0.5}O_2$ (y ~ 1) and a $Li_{2-y}Ni_{0.5}Mn_{0.5}O_2$ (y ~ 0.2) phase, which is nearly fully lithiated in Figure 3b

(19) Marezio, M.; Remeika, J. P. *J. Chem. Phys.* **1996**, *44*, 3348.
(20) Connelly, N. G.; Geiger, W. E. *Chem. Rev.* **1996**, *96*, 877.
(21) Rieck, H.; Hoppe, R. *Z. Anorg. Allg. Chem.* **1972**, *392*, 193.
(22) Dahn, J. R.; von Sacken, U.; Michal, C. A. *Solid State Ionics* **1990**, *44*, 87.
(23) David, W. I. F.; Goodenough, J. B.; Thackeray, M. M.; Thomas, M. G. S. R. *Rev. Chem. Miner.* **1983**, *20*, 636.

Table 1. Lattice Parameters for Various $Li_xNi_{0.5}Mn_{0.5}O_2$ Compounds from Chemical Lithiation Experiments and In Situ XRD Experiments

sample	description-notes	crystal	*Z*	*a* (Å)	*c* (Å)	vol. (Å^3)
$LiNi_{0.5}Mn_{0.5}O_2$[a]	powder, as-prepared	$R\bar{3}m$	3	2.881(1)	14.278(2)	102.61(2)
$Li_2Ni_{0.5}Mn_{0.5}O_2$[b]	chemically lithiated product	$P\bar{3}m1$	1	3.130(4)	5.196(19)	44.09(18)
$Li_{2-y}Ni_{0.5}Mn_{0.5}O_2$ ($y \sim 0.2$)	air-oxidized (2 h)	$P\bar{3}m1$	1	3.143(2)	5.002(7)	42.80(7)
$LiNi_{0.5}Mn_{0.5}O_2$	air-oxidized (10 h)	$R\bar{3}m$	3	2.905(2)	14.48(2)	105.9(2)
$0.95LiMn_{0.5}Ni_{0.5}O_2 \cdot 0.05Li_2TiO_3$	ref 9	$R\bar{3}m$	3	2.877(1)	14.284(2)	102.39(1)
$LiNi_{0.5}Mn_{0.5}O_2$[a]	A; as-built, in cell before charge	$R\bar{3}m$	3	2.880(1)	14.272(12)	102.5(1)
$Li_xNi_{0.5}Mn_{0.5}O_2$ ($x \sim 0.2$)	B; first charge, 4.5 V in cell	$R\bar{3}m$	3	2.830(4)	14.29(4)	99.2(3)
$Li_xNi_{0.5}Mn_{0.5}O_2$ ($x \sim 0.8$)	C; first discharge, 2.0 V in cell	$R\bar{3}m$	3	2.879(2)	14.30(2)	102.6(2)
$Li_xNi_{0.5}Mn_{0.5}O_2$ ($x \sim 1$)	D; first discharge, 1.5 V in cell	$R\bar{3}m$	3	2.908(1)	14.37(1)	105.3(1)
$Li_xNi_{0.5}Mn_{0.5}O_2$ ($x \sim 1.45$)	E; first discharge, 1.0 V in cell	$P\bar{3}m1$	1	3.136(29)	5.19(15)	44.2(14)
$Li_xNi_{0.5}Mn_{0.5}O_2$ ($x \sim 1$)	F; second charge, 2.2 V in cell	$R\bar{3}m$	3	2.891(2)	14.24(1)	103.1(2)
$Li_xNi_{0.5}Mn_{0.5}O_2$ ($x \sim 0.27$)	G; second charge, 4.5 V in cell	$R\bar{3}m$	3	2.830(5)	14.29(5)	99.1(3)
$LiNi_{0.5}Mn_{0.5}O_2$	ref 7 as-prepared	$R\bar{3}m$	3	2.892	14.301	103.58
$LiNi_{0.5}Mn_{0.5}O_2$	ref 8[c] as-prepared	$R\bar{3}m$	3	2.890	14.298	103.42
$LiNi_{0.5}Mn_{0.5}O_2$	ref 24; initial cell, scan 1 (H1 phase)	$R\bar{3}m$	3	2.895	14.311	103.87
$Li_{1-x}Ni_{0.5}Mn_{0.5}O_2$	ref 24; 4.7 V cell scan 10 (H2 phase)	$R\bar{3}m$	3	2.839	14.428	100.71
$Li[Li_{0.06}Ni_{0.42}Mn_{0.53}]O_2$	ref 30 (i.e., $x = 5/12$; initial from Figure 5)	$R\bar{3}m$	3	2.877	14.277	102.34
$[Li_{0.06}Ni_{0.42}Mn_{0.53}]O_{1.916}$ (oxygen loss structure)	ref 30 (i.e., $x = 5/12$; 4.8 V from Table 2)	$R\bar{3}m$	3	2.8478(3)	14.1958(30)	99.7

[a] $Li_{0.906}Ni_{0.506}Mn_{0.494}O_2$ (ICP-AES). [b] $Li_{1.88}Ni_{0.514}Mn_{0.486}O_2$ (ICP-AES). [c] Estimated from Figure 2 in ref 8.

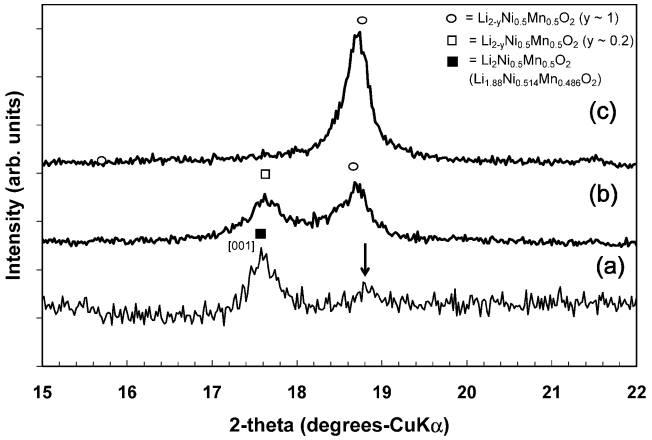

Figure 3. XRD patterns (blow-up region 15−22° 2θ) of layered $Li_xNi_{0.5}Mn_{0.5}O_2$ oxides: from bottom to top, (a) chemically lithiated $Li_2Ni_{0.5}Mn_{0.5}O_2$ ($Li_{1.88}Ni_{0.514}Mn_{0.486}O_2$) under a Be foil cover, (b) sample in (a), after 2 h of air exposure; and (c) sample in (a) after 10 h of air exposure.

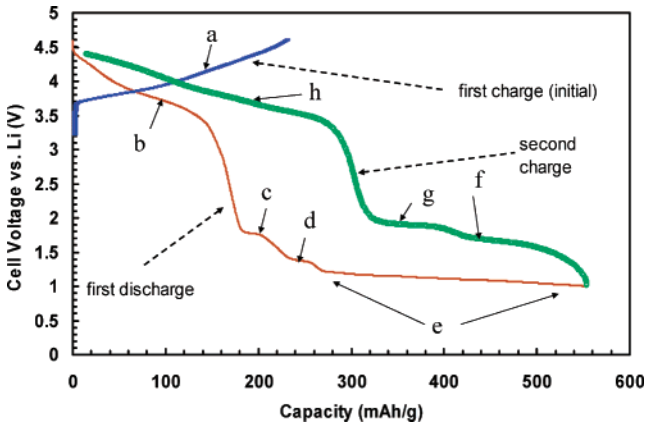

Figure 4. Voltage profile of a Li/$Li_xNi_{0.5}Mn_{0.5}O_2$ cell between 4.6 and 1.0 V at room temperature; current = 3.6 mA/g (C/150). See Table 2 for label identification (a−h) and description.

(full 2θ range in Figure 1c). From Rietveld analysis of the XRD patterns, it appears that a small range of solid solution exists between the fully lithiated end-product $Li_2Ni_{0.5}Mn_{0.5}O_2$ and $Li_{2-y}Ni_{0.5}Mn_{0.5}O_2$ for $0 \le y \le 0.2$. The lattice parameters of $Li_{1.8}Ni_{0.5}Mn_{0.5}O_2$ ($y = 0.2$) are $a = 3.143(2)$ Å and $c = 5.002(7)$ Å; the corresponding volume of the unit cell is 42.80 Å^3. The extruded lithium at the particle surface subsequently reacts with CO_2 in the air to form Li_2CO_3, leaving behind, after 10 h of exposure to air, a reoxidized product with a stoichiometry close to the parent $LiNi_{0.5}Mn_{0.5}O_2$ material, as shown in Figure 3c (full 2θ range in Figure 1d).

It is interesting to note that the lithiation and air-delithiation reactions described above do not produce any Mn(III)-associated secondary phases, such as the commonly observed Li−Mn−O spinel-type phases. Furthermore, by XRD no obvious Ni and/or Mn displacement reactions occur during the chemical reaction of $LiNi_{0.5}Mn_{0.5}O_2$ with lithium naphthalide. The retention and robustness of the layered $Ni_{0.5}Mn_{0.5}O_2$ framework is a unique feature of the reaction, even though the material after reoxidation becomes less crystalline.

The XRD data from both chemical (top section) and electrochemical Li insertion and extraction (middle section) are summarized in Table 1. For comparison, in Table 1 (bottom section) are the crystallographic values reported in the literature by Ohzuku and Makimura,[7] Lu et al.,[8] and Yang et al.[24] on their layered $Li_xNi_{0.5}Mn_{0.5}O_2$ ($0 < x \le 1$) systems. There is some variance in the reported unit-cell parameters for these systems that may be attributed to slight differences in lithium, nickel, and manganese compositions and the different numeric methods used to calculate the lattice parameters.

3.2. Electrochemical Voltage Profile of Layered Li/$Li_xNi_{0.5}Mn_{0.5}O_2$ Cells. In Figure 4 a charge−discharge curve is shown for the Li/$Li_xNi_{0.5}Mn_{0.5}O_2$ cell over a large voltage window (4.6−1.0 V). The coin cell was cycled at room temperature and at a slow rate (3.6 mA/g, C/150) to facilitate electrode equilibration and to negate overpotential effects in the cell. The specific electrode capacity is very high and yet the reversibility still was quite good within this potential range. This cell was initially charged to 4.6 V and yielded 229 mA·h/g capacity. On the basis of the initial lithium content

(24) Yang, X.-Q.; McBreen, J.; Yoon, W.-S.; Grey, C. *Electrochem. Commun.* **2002**, *4*, 649.

in the sample, this capacity is about 90% of the theoretical value. The cell was subsequently discharged to 1.0 V, followed by a recharge back to 4.4 V; the electrode provided 554 mA·h/g on discharge and 540 mA·h/g on charge at this slow rate. The cycling/voltage profile was very similar to that reported previously for the related $0.95LiMn_{0.5}Ni_{0.5}O_2 \cdot 0.05Li_2TiO_3$ system.[13,14]

In the most simplest terms, and assuming that complete extraction and insertion of lithium is possible, the idealized electrochemical (and chemical) reactions would be (1)

$$[\,](Ni_{0.5}Mn_{0.5})O_2 + Li \xleftrightarrow{(a)} Li(Ni_{0.5}Mn_{0.5})O_2 \pm Li \xleftrightarrow{(b)} Li_2(Ni_{0.5}Mn_{0.5})O_2 \quad (1)$$

Two sequential reactions, (1a) and (1b), in principle, represent the two successive reactions that occur at voltages approximately between 4.6 and 1.0 V versus metallic Li. Overall, the theoretical capacity over both sets of reactions is 560 mA·h/g, delivered as 280 mA·h/g in each sequence where reaction 1a involves a multielectron-transfer reaction associated with the $Ni^{4+/2+}$ redox couple and reaction 1b the multielectron-transfer reaction associated with the $Mn^{4+/2+}$ redox couple. The overall capacity thus observed in the first discharge (554 mA·h/g) to 1.0 V in Figure 4 was found to be 99% of the theoretical for the full reaction in (1).

The reaction represented in (1b) is, of course, ideal. Lithium insertion into metal oxides at lower voltages accompanied by reduction to divalent metal ions is known in previous battery studies, particularly for Co_3O_4[25] and Mn_3O_4[26] spinel oxides. Recently, examinations of electrochemical reactions of lithium specifically with divalent metal oxides such as CoO, MnO, and NiO have been reported.[27] These reactions involve displacement of the metal ions from the structure to form lithium oxide (lithia, Li_2O) and elemental metal. The relative voltage of the displacement reaction depends on thermodynamic properties of the reaction but, in practice, is influenced by kinetic factors.

Such a displacement reaction may be written for the layered $Li_2Ni_{0.5}Mn_{0.5}O_2$ oxide as follows in eq 2. The theoretical capacity for the reaction is 261 mA·h/g.

$$Li_2(Ni_{0.5}Mn_{0.5})O_2 + Li \rightarrow 1.5Li_2O + 0.5Ni + 0.5MnO \quad (2)$$

If this reaction occurs in cells, it would obviously contribute additional capacity at the low-end voltage cutoff. Depending on the particle size, some electrochemical reversibility could be possible, analogous to nanosized CoO.[28]

A number of plateaus are observed in the voltage profile, which we believe correspond to electrode kinetic factors and diffusional overvoltages associated with a combination of the reactions in eqs 1b and 2. Also, the electrode microstructure morphology can influence the reaction pathway for insertion versus displacement reactions.[29] A summary of the voltages and the capacities associated with these plateaus and features are presented in Table 2 and are marked in Figure 4. In general, many of the cells that have been cycled show this representative profile shape over the full voltage window when conducted at a slow current rate and within the first few charge−discharge cycles. However, these plateaus and voltage profile features can change their lengths (capacities) and corresponding voltages depending, particularly, on the cathode sample history, both in the as-prepared state and under cycling conditions. Some discussion of these processes is explained in more detail below from the physical and structural characterization studies.

Table 2. Voltage Profile Summary for $Li/Li_xNi_{0.5}Mn_{0.5}O_2$ Cells

voltage profile marking	voltage range (V)	specific capacity (mA·h/g)	voltage profile marking	voltage range (V)	specific capacity (mA·h/g)
a	3.25−4.6	228	e	1.2−1.0	278
b	4.6−1.8	184	f	1.0−1.85	157
c	1.8−1.42	50	g	1.85−3.0	103
d	1.42−1.2	42	h	3.0−4.4	280

3.3. In Situ XRD of $Li/Li_xNi_{0.5}Mn_{0.5}O_2$ Cells. To probe the reaction details presented in eqs 1 and 2 in an operating electrochemical cell, the $LiNi_{0.5}Mn_{0.5}O_2$ material was cycled in a special X-ray transparent "coffee-bag" cell. The material was first charged to 4.5 V, delivered 199 mA·h/g, then discharged to 1.0 V (347 mA·h/g), and recharged back to 4.5 V (325 mA·h/g). The XRD patterns are shown in Figure 5a sequentially stacked in patterns A−G (lowest to highest stacked profile). Figure 5b also provides the blow-up of the XRD region between about 15 and 22° 2θ. The lattice parameter calculations are summarized in Table 1 (middle section).

The associated capacities between the stacked XRD patterns are the following: A−B, 199 mA·h/g; B−C, 170 mA·h/g; C−D, 54 mA·h/g; D−E, 126 mA·h/g; E−F, 93 mA·h/g; F−G, 232 mA·h/g. The phases are consistent with the interpretation that the reaction at upper voltage (4.5−2.0 or 1.5 V vs Li) is a single-phase insertion/extraction reaction, whereas the lower voltage reaction (1.5−1.0 V vs Li) is associated primarily with a two-phase reaction between $LiNi_{0.5}Mn_{0.5}O_2$ and its electrochemically lithiated product $Li_2Ni_{0.5}Mn_{0.5}O_2$. There is no XRD evidence of Ni or Mn reduction to the metal by displacement from the oxide (eq 2) in the low-voltage two-phase region after cycling at higher voltage. However, such displacement reaction(s) could tend to produce materials that are extremely finely dispersed, located only at grain boundaries, and are difficult to identify by XRD.[28]

Assuming all of the charge passed is lithium cation extraction and the starting composition is fixed by the ICP-AES analysis, then the initial charge from OCV to 4.5 V gives a calculated composition of $Li_{0.206}Ni_{0.506}Mn_{0.494}O_2$ ($x \sim 0.2$; approximate $Li_{0.2}Ni_{0.5}Mn_{0.5}O_2$ composition). As is evident from the monotonic shift in the peaks during the charge (Figure 5a,b, pattern A to pattern B), lithium extraction is accompanied by a contraction of the oxygen lattice in response to the

(25) Thackeray, M. M.; Baker, S. D.; Adendorff, K. T.; Goodenough, J. B. *Solid State Ionics* **1985**, *17*, 175.
(26) Goodenough, J. B.; Thackeray, M. M.; David, W. I. F.; Bruce, P. G. *Rev. Chim. Miner.* **1984**, *21*, 435.
(27) Poizot, P.; Laruelle, S.; Grugeon, S.; Tarascon, J.-M. *J. Electrochem. Soc.* **2002**, *149*, A1212.
(28) Poizot, P.; Laruelle, S.; Grugeon, S.; DuPont, L.; Tarascon, J.-M. *Nature* **2000**, *407*, 496.
(29) Larcher, D.; Sudant, G.; Leriche, J.-B.; Chabre, Y.; Tarascon, J.-M. *J. Electrochem. Soc.* **2002**, *149*, A234.

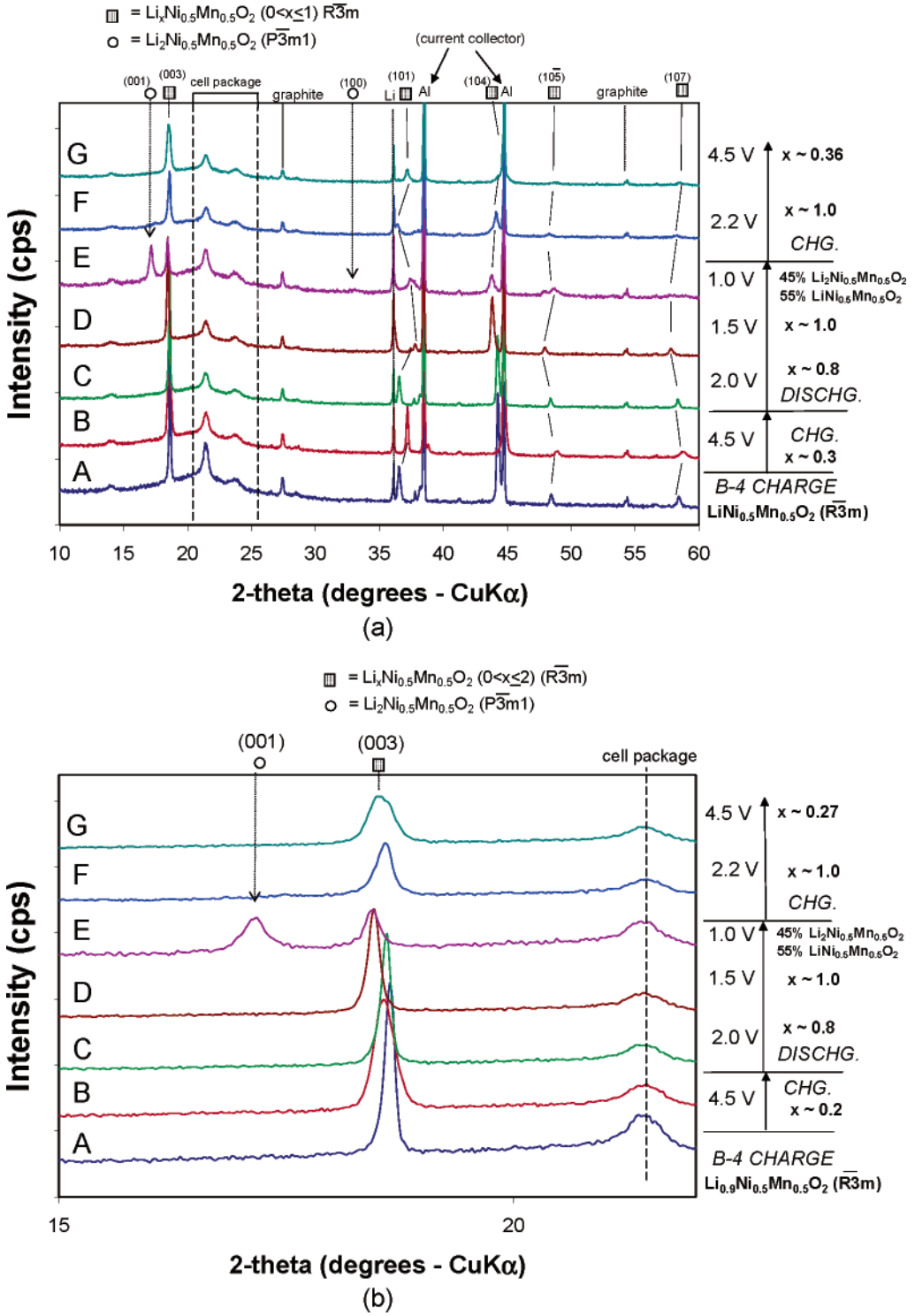

Figure 5. (a) In situ XRD patterns of the Li/$Li_xNi_{0.5}Mn_{0.5}O_2$ coffee-bag cell equilibrated at potentials between 4.5 and 1.0 V: from bottom to top, (A) OCV before charge, (B) 4.5 V at top of charge, (C) 2.0 V during discharge, (D) 1.5 V during discharge, (E) 1.0 V during discharge, (F) 2.2 V during second charge, and (G) 4.5 V at top of second charge. Voltages as marked were the cutoff values prior to cell equilibration. Compositions are labeled and marked as indicated and are estimated based on the charge passed in the electrochemistry. (b) Blow-up region 15−22° 2θ; same identifiers marked in (a).

increase in the average oxidation state of the nickel and decrease in Ni−O average bond length. This finding is consistent with a recent in situ Li coin cell (Be window) XRD study on the closely related composition Li-$[Ni_xLi_{1/3-2x/3}Mn_{2/3-x/3}]O_2$ (x = 5/12; elemental analysis $Li[Li_{0.06}Ni_{0.42}Mn_{0.53}]O_2$) conducted by Lu and Dahn up to 4.4 V.[30] From the lattice parameter calculation, the unit-cell volume decreases by 3.2% from 102.5 to 99.2 Å (c/a = 5.049) for the delithiated $Li_{0.2}Ni_{0.5}Mn_{0.5}O_2$ oxide at 4.5 V (Table 1 and Figure 5a,b, pattern B).

It should also be noted that different in situ cycling XRD (synchrotron source) results were obtained on a

(30) Lu, Z.; Dahn, J. R. *J. Electrochem. Soc.* **2002**, *149*, A815.

$Li_xNi_{0.5}Mn_{0.5}O_2$ electrode charged to higher voltages as reported by Yang et al.[24] They, instead, identified a clear hexagonal (H1) to hexagonal (H2) phase change in the material above 4.5 V in their cell. For comparison, their unit-cell values are also shown in Table 1 in this paper. Because of the limited number of peaks observed in our study and the limited resolution of our XRD patterns, these Rietveld profile refinements were confined to a single hexagonal phase initially defined at the beginning of the first charge. However, it is worth commenting that we do observe some XRD peak broadening in the pattern collected, particularly at 4.5 V top of charge in both the first and second cycle, which may be related to the onset formation of a second hexagonal phase (H2) as identified by Yang et al. at voltages above 4.5 up to 4.7 V.[24] Finally, in the refinement, we did not observe a large shrinkage in the *c* axis of the unit cell for the electrode at 4.5 V (199 mA·h/g; $Li_{0.2}Ni_{0.5}Mn_{0.5}O_2$). It was discussed elsewhere that a large decrease in the *c* axis could be attributed to structural instability and oxygen loss in the material. This was observed at higher voltages to 4.8 V in the in situ XRD study on $Li[Li_{0.06}Ni_{0.42}Mn_{0.53}]O_2$ by Lu and Dahn.[30]

As the $Li/Li_{0.2}Ni_{0.5}Mn_{0.5}O_2$ cell is discharged from 4.5 to 2.0 V, the lattice expands back to almost its original value, yielding a $Li_xNi_{0.5}Mn_{0.5}O_2$ ($x \sim 0.8$) structure with an overall cell volume of 102.6 Å ($c/a = 4.967$; Table 1 and Figure 5a,b, pattern C). Continuing the discharge from 2.0 V to a lower voltage of 1.5 V gives extra capacity of 54 mA·h/g and causes slight lattice expansion as shown in the slight shift of the (003) peak to lower 2θ (Table 1 and Figure 5a,b, pattern D). This observation is consistent with the interpretation that the nickel metal cation is reduced completely to Ni^{2+} at a final voltage of 1.5 V. The voltage for complete electrochemical reduction required to drive the nickel completely to its divalent state is thus lower than the 3.0 or 2.0 V cutoff that normally is used to cycle $Li/LiNi_{0.5}Mn_{0.5}O_2$ cells.[7−8,10,12] It should also be noted that the calculated average oxidation state of Ni in the as-prepared sample was 2.2^+ and is consistent with the higher 3.6-V open-circuit voltage of the cell prior to its first charge. Cycling voltage windows of 4.5 to 2.0 V may therefore limit the complete electrochemical reduction of the nickel at the end of discharge.

Below 1.5 V, a peak due to the $Li_2Ni_{0.5}Mn_{0.5}O_2$ structure appears and is shown at 1.0 V (Table 1 and Figures 5a,b, pattern E) as evidenced by a large (001) reflection identified at ca. 17° 2θ. In contrast to our work, the formation of the $Li_2Ni_{0.5}Mn_{0.5}O_2$ phase was not observed at low voltages in the in situ XRD data obtained by Yang et al.[24] However, it should be noted that the difference in results could be associated with nonequilibrium effects and higher impedance in the cell cycled at a higher current rate by Yang compared to the work presented here.

Taking the additional capacity as associated with the insertion of additional Li into the layer yields an approximate composition of $Li_{1.45}Ni_{0.5}Mn_{0.5}O_2$ or, more accurately, 55% $LiNi_{0.5}Mn_{0.5}O_2$ and 45% $Li_2Ni_{0.5}Mn_{0.5}O_2$. This phase grows at the expense of the $LiNi_{0.5}Mn_{0.5}O_2$ phase by causing an intensity decrease of the (003) peak at ca. 19° 2θ. Very related and similar lithiated phases for the $LiNi_{0.5}Mn_{0.5}O_2$ solid-solution separated end-members of Li_2NiO_2 and Li_2MnO_2 were, respectively, reported over 10 years ago by Dahn et al. [22] and almost 20 years ago by David et al.[23]

Reversing the current in the cell and recharging from 1.0 V back up to 4.5 V results in the XRD patterns of the hexagonal phase $LiNi_{0.5}Mn_{0.5}O_2$ reappearing represented at 2.2 V (Table 1, Figure 5a,b, pattern F), followed by the XRD pattern of $Li_xNi_{0.5}Mn_{0.5}O_2$ ($x \sim 0.27$) at top of charge at 4.5 V (Table 1, Figure 5a,b, pattern G). With a qualitative comparison of Figure 5a,b, pattern A, collected prior to the cell's initial charge, with that of Figure 5a,b, pattern G, after cycling down to 1.0 V, one can see that some of the crystallinity of the powder is lost. However, no new phases or peaks appear in this experiment. It is possible that repetitive cycling down to the $Li_2Ni_{0.5}Mn_{0.5}O_2$ phase could lead to excessive particle fracturing due to the roughly 20% crystal volume increase associated with the $LiNi_{0.5}Mn_{0.5}O_2 + Li \rightarrow Li_2Ni_{0.5}Mn_{0.5}O_2$ reaction. An eventual loss of particle−particle contact and electronic isolation as a result of this phase change would hinder its galvanostatic reversibility and usefulness over the full voltage window of cycling in practical cells.

It is important to place in context the complexities that arise that are associated with overpotential complications/conditions in the electrochemistry. The cell voltage required to drive the $LiNi_{0.5}Mn_{0.5}O_2 + Li \rightarrow Li_2Ni_{0.5}Mn_{0.5}O_2$ electrochemical reaction is substantially different if the cell is first charged to 4.5 V, and not, instead, discharged first to 1.5 V or lower to 1.0 V. In the latter case the discharge reaction to insert additional Li into the "filled" layer occurs about 0.5 V higher, corresponding to a smaller overpotential for the process.[14] While at this point the interpretation is speculative, the higher cell impedance or excessive cell polarization at the lower voltage reaction may be a consequence of slow Li diffusion kinetics that have been predicted for layered $LiMO_2$ oxides (M = Co) that have a rock-salt composition and are fully filled with lithium in the layer.[31] The slow kinetics might further be a result of electrode microstructure morphology changes during cycling, particularly at low voltages.[29] Additional detailed studies are required to determine underlying causes.

Sluggish electrode kinetics would translate into a greater overpotential needed in the cell to drive the second Li into the layer with a simultaneous shear of the oxygen planes. As a result, the voltage of the reaction would be driven lower compared to first discharging a fresh $LiNi_{0.5}Mn_{0.5}O_2$ electrode. The electrode as-prepared is thus envisioned as having a more pure layered structure with no transition metal cations contaminating the Li layer. For example, in the pure $LiNiO_2$ system, the type of synthesis method used has been known to cause the appearance of divalent Ni^{2+} occupation onto the Li layer site.[32] In addition, the appearance of Ni^{2+}on the lithium site also results in disordered materials and associated poor electrochemical performance.[33]

(31) Van der Ven, A.; Ceder, G. *J. Power Sources* **2001**, *97−98*, 529.
(32) Bianchi, V.; Caurant, D.; Baffier, N.; Belhomme, C.; Chappel, E.; Chouteau, S.; Bach, S.; Pereira-Ramos, J. P.; Sulpice, A.; Wilmann, P. *Solid State Ionics* **2001**, *140*, 1.
(33) Riemers, J. N.; Dahn, J. R. *Phys. Rev., B: Condens. Matter* **1992**, *46*, 3236.

Table 3. Nickel and Manganese X-ray Absorption Near-Edge Spectroscopy (XANES) Results

sample	Ni main K edge E_m (eV) ($\mu x = 0.5$)	Mn main K edge E_m (eV) ($\mu x = 0.5$)	Mn K pre-edge E_p (eV) ($\mu x = 0.25$)
$LiNi_{0.5}Mn_{0.5}O_2$[a] as-prepared	8342.90	6552.99	6548.72
$Li_{0.27}Ni_{0.5}Mn_{0.5}O_2$ charged	8345.20	6551.93	6549.12
$Li_2Ni_{0.5}Mn_{0.5}O_2$[b] chemical lithiated	8342.4	6547.76	6545.40
Ni	8340.51		
NiO	8342.26		
$LiNiO_2$	8344.67		
Mn		6540.63	6538.11
MnO		6544.01	6542.77
Mn_2O_3		6549.12	6546.82
Li_2MnO_3		6553.00	6548.92

[a] $Li_{0.906}Ni_{0.506}Mn_{0.494}O_2$ (ICP-AES). [b] $Li_{1.88}Ni_{0.514}Mn_{0.486}O_2$ (ICP-AES).

It would be difficult to form Li_2MO_2 (M = Ni, Co, and/or Mn) type structure if M cations are located in the tetrahedral sites. Divalent Ni^{2+} located at the surface of electrochemically delithiated layered $LiNi_{0.8}Co_{0.2}O_2$ has been observed from high-resolution electron microscopy (HREM) and X-ray absorption spectroscopy studies.[34] The Ni^{2+} migration to adjacent layers also predominates the Li_xNiO_2 system during phase changes at small values of x at top of charge, where electrostatic repulsion with lithium cations is smaller.[35] For the layered $Li_xNi_{0.5}Mn_{0.5}O_2$ during discharge to lower voltages where additional lithium is being pushed into the lithium layer ($x > 1$), a strong electrostatic repulsion builds and site blockage to the entering lithium cations occurs if the divalent Ni^{2+} already resides in the layer. This would in effect cause slower electrochemical reaction kinetics for the second lithium ion to insert or diffuse into the Li layer with resultant higher cell polarization or impedance and a higher overpotential.

3.4. XAS of $Li_xNi_{0.5}Mn_{0.5}O_2$ Compounds. A detailed description of the charge compensation mechanism involved at low voltages for $Li(Ni_{0.5}Mn_{0.5})O_2 \leftrightarrow Li_2(Ni_{0.5}Mn_{0.5})O_2$ transition was reported previously in an XAS in situ cell study.[14] To add to the knowledge and data for this system, additional results from ex situ XAS work on powders from the series: $Ni_{0.5}Mn_{0.5}O_2-LiNi_{0.5}Mn_{0.5}O_2-Li_2Ni_{0.5}Mn_{0.5}O_2$ was analyzed in this study. The Ni and Mn K edge data and results are summarized in Table 3.

Figure 6a shows the Ni K edge XANES spectra collected for the three powders of interest. A main energy shift (E_m) of about 2 eV per oxidation state unit for Ni was fit qualitatively at half-height of the normalized edge step ($\mu x = 0.5$).[36] The standards measured for this fitting were Ni metal, NiO, and $LiNiO_2$. The edge position for Ni in the as-prepared $LiNi_{0.5}Mn_{0.5}O_2$ was 8342.90 eV. This value is shifted to slightly higher energy compared to that of the NiO (Ni^{2+}) standard (8342.26 eV), indicating that the oxidation state of Ni

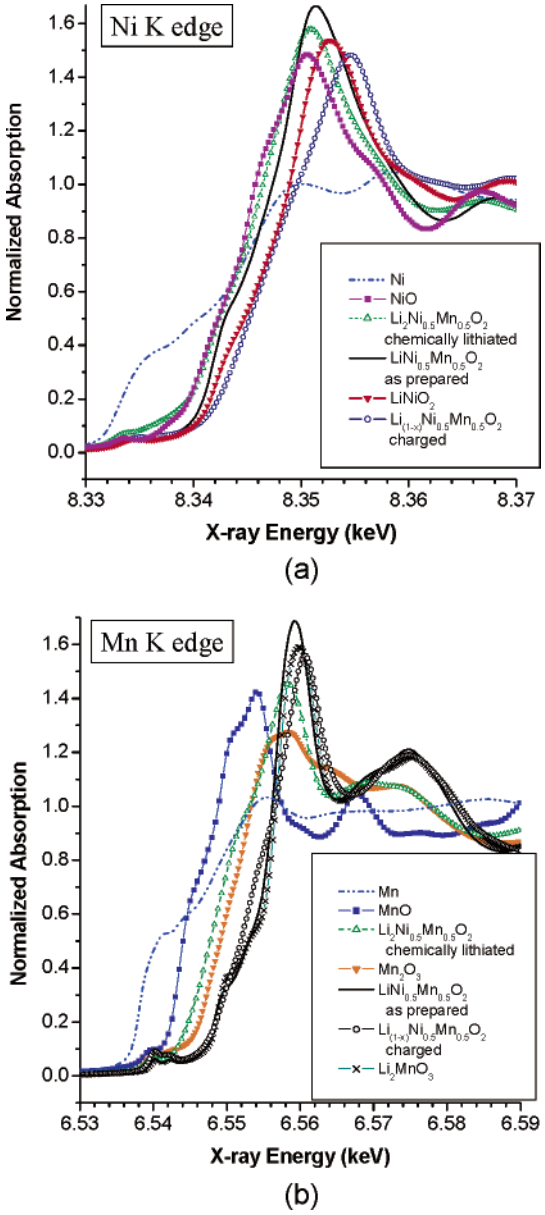

Figure 6. Calibrated and normalized XANES data: (a) Ni K edge and (b) Mn K edge. Reproducibility of the calibration is ±0.1 eV. Curves are identified as marked.

in the as-prepared sample of $LiNi_{0.5}Mn_{0.5}O_2$ is about 2.25 ± 0.1. Assuming all Mn^{4+} in the sample, this result agrees very well with the Li-deficient $Li_{0.906}Ni_{0.506}Mn_{0.494}O_2$ composition determined from ICP-AES measurements. The edge position for standard $LiNiO_2$ (Ni^{3+}) was measured at 8344.67 eV.

After charge of $LiNi_{0.5}Mn_{0.5}O_2$ to 4.6 V, the Ni edge shifts by 1.52 eV to higher energy (8345.20 eV) and suggests that the Ni metal center is oxidized to some value between +3 and +4, but closer to +3 at approximately +3.2. It is important to note, however, that XANES presents only an average composition for the sample. Thus, the formal oxidation state of Ni in this case could either be defined as a 40/60 ratio of +2/+4, or in another interpretation, delocalized fully being +3.2. Curve fitting and analysis of the EXAFS data is in progress[37] and it will be informative to compare our

(34) Abraham, D.; Twesten, R. D.; Balusubramanian, M.; Petrov, I.; McBreen, J.; Amine, K. *Electrochem. Commun.* **2002**, *4*, 620.
(35) Ohzuku, T.; Ueda, A.; Nagayama, M. *J. Electrochem. Soc.* **1997**, *144*, 3117.
(36) Mansour, A. N.; McBreen, J.; Melendres, C. A. *J. Electrochem. Soc.* **1999**, 146, 2799.
(37) Kropf, A. J.; Johnson, C. S.; Kim, J.-S.; Thackeray, M. M. Unpublished data, 2002.

results on the short-range order and bond lengths in this system to the findings by Yoon et al.[38]

Interestingly, the specific capacity for this cell charged to 4.6 V ex situ was 178 mA·h/g and equates to a nominal composition of $Li_{0.27}Ni_{0.5}Mn_{0.5}O_2$ (Li = 0.63) based on the charge passed and the analyzed starting material composition. In this case the sample Ni K edge shift should have been observed at a higher energy equivalent to a formal oxidation state of 3.46 or 27% Ni +2 and 73% Ni +4. More work is required to understand this discrepancy. In addition, it is reasonable to expect that the delithiated $Li_{0.2}Ni_{0.5}Mn_{0.5}O_2$ sample may have reacted with moisture during sample handling and measurement despite rigors to control the environment. In this case the oxidized Ni would become subsequently reduced in the sample due to a side reaction with water.

For the sample that was chemically lithiated to a nominal stoichiometry of $Li_{1.88}Ni_{0.5}Mn_{0.5}O_2$, the Ni K edge (8342.40 eV) is only slightly shifted down in energy from 8342.90 eV observed in the as-prepared $Li_{0.9}Ni_{0.5}Mn_{0.5}O_2$. This indicates slight chemical reduction of the average Ni oxidation state from +2.2 (as-prepared state) to nearly +2. The position of the Ni K edge was within 0.2 eV of the NiO standard at 8342.26 eV.

The extra intensity in the pre-edge region of the XANES for the chemically lithiated $Li_{1.88}Ni_{0.5}Mn_{0.5}O_2$ indicates that a small amount of Ni metal may have been formed. Fitting the XANES to a linear combination of all three paths, Ni metal, NiO, and the as-prepared $Li_{0.9}Ni_{0.5}Mn_{0.5}O_2$, results in a fit showing that 8 ± 3% of the Ni has a lowered average oxidation state and potentially has become Ni metal. This observation could suggest that eq 2, a Ni metal displacement reaction from $Li_2Ni_{0.5}Mn_{0.5}O_2$ (or $LiNi_{0.5}Mn_{0.5}O_2$), may occur in the electrode at low cell voltages.

The XANES for the Mn K edge is also presented in Figure 6b. A main energy shift (E_m) of about 3.8 eV per oxidation state unit for Mn was fit quantitatively at half-height of the normalized edge step ($\mu x = 0.5$).[36] The standards measured for this edge fit were Mn metal, MnO, Mn_2O_3, and Li_2MnO_3. Note that the trend of the Mn K edge position changes in the series $Ni_{0.5}Mn_{0.5}O_2$−$LiNi_{0.5}Mn_{0.5}O_2$−$Li_2Ni_{0.5}Mn_{0.5}O_2$ track oppositely to that of the Ni K edge (Figure 6a).

For the sample taken out of the charged cell the Mn edge position ($\mu x = 0.5$) was 6551.93 eV compared to that of the as-prepared starting material $Li_{0.9}Ni_{0.5}Mn_{0.5}O_2$ powder (6552.99 eV). The edge position at quarter-height of the normalized edge step ($\mu x = 0.25$), however, indicates a slightly higher energy shift but is essentially the same as that of the as-prepared $Li_{0.9}Ni_{0.5}Mn_{0.5}O_2$ sample or the Li_2MnO_3 standard within the experimental error of ±0.1 eV. Qualitatively, the XANES spectra for the as-prepared $Li_{0.9}Ni_{0.5}Mn_{0.5}O_2$ material look very similar in shape to the Li_2MnO_3 standard, and thus the binding energy and the local order are estimated to be nearly equivalent and representative of tetravalent Mn^{4+} in a layered Mn distribution similar to those of $Li[Li_{0.33}Mn_{0.67}]O_2$ (Li_2MnO_3).

An edge shift to lower energy at 6547.76 eV is observed for the $Li_{1.88}Ni_{0.5}Mn_{0.5}O_2$ sample that was lithiated chemically. The shift occurs beyond that of Mn^{3+} (Mn_2O_3; 6549.12 eV) and is more similar to the MnO standard (6544.01 eV), which is divalent Mn^{2+}. Again, it is noted that the sample handling did not rigorously exclude air from the sample, and possibly some oxidation from O_2 of the sample had occurred during measurement at the beamline, thus shifting the edge to slightly higher eV. If we look exactly at the metal mole ratio in the lithiated product as 1.88:0.514:0.486 Li:Ni:Mn and assume that the oxygen content is 2, then the experimentally calculated average oxidation state of Mn in this sample is 2.25 and agrees with a slightly higher energy shift from pure divalent 2.0. It should be noted that the likelihood of reactivity to air and/or moisture is high and was also observed in the ex situ XRD experiments taken on the lithiated $Li_{1.88}Ni_{0.5}Mn_{0.5}O_2$ sample.

Thus, to summarize, the XAS data are empirically consistent with eq 1 and may be explained by the following compositions: $Ni_{0.5}Mn_{0.5}O_2$−$LiNi_{0.5}Mn_{0.5}O_2$−$Li_2Ni_{0.5}Mn_{0.5}O_2$ where the metal oxidation states are locally $Ni^{4+}Mn^{4+}$−$Ni^{2+}Mn^{4+}$−$Ni^{2+}Mn^{2+}$. It also should be noted that a cursory analysis of the EXAFS data for both the Ni and Mn K edges for the $Li_2Ni_{0.5}Mn_{0.5}O_2$ powder possibly indicate some formation of metallic Ni (8 ± 3%) that would be present from the product in eq 2.[29,37]

4. Conclusions

Synthesis and characterization analysis for the lithiated and delithiated products of $Li_xNi_{0.5}Mn_{0.5}O_2$ ($0 < x \leq 2$) were conducted. XRD was used for phase examination, and XAS was used to determine the Ni and Mn formal oxidation states. These results, together with electrochemical cycling data, suggest that $LiNi_{0.5}Mn_{0.5}O_2$ layered electrodes operate predominantly off two-electron redox couples, Ni^{4+}/Ni^{2+} and Mn^{4+}/Mn^{2+}, between 4.5 and 2.0 V ($0 < x \leq 1$) and between 2.0 and 1.0 V ($1 < x \leq 2$) versus metallic Li, respectively. However, the location of the voltages for the reactions can change depending on the exact composition of the electrode, which can be altered by past sample history and prior cycling conditions. The electrochemical reaction between Li and $LiNi_{0.5}Mn_{0.5}O_2$ to form $Li_2Ni_{0.5}Mn_{0.5}O_2$ at low voltage is sensitive to Li/metal (Ni and/or Mn) site mixing. Thus, the greater the mixing of Ni and/or Mn within the Li layer (site disorder), the greater the electrostatic repulsive forces against further additional Li insertion.

The retention of a stable layered oxide framework and the apparent absence of Jahn−Teller ions Ni^{3+} and Mn^{3+} in the high- or low-voltage region is believed to contribute to the excellent structural and electrochemical stability of these electrodes. The $LiNi_{0.5}Mn_{0.5}O_2$ is shown by XRD to form a quasi-stable dilithium compound, $Li_2Ni_{0.5}Mn_{0.5}O_2$ (Li_2MO_2); the structure is hexagonally close-packed (space group $P\bar{3}m1$). The reaction is reversible, both chemically and electrochemically.

The cycling behavior of $Li/LiNi_{0.5}Mn_{0.5}O_2$ cells was studied over a large voltage window (4.6−1.0 V) with a very slow current rate (C/150). The results show that rechargeable capacities >500 mA·h/g could be obtained. The very large discharge capacities yielded at low voltages are the result of the formation of a portion of highly lithiated material $Li_2Ni_{0.5}Mn_{0.5}O_2$ together with

(38) Yoon, W. S.; Paik, Y.; Yang, X.-Q.; Balasubramanian, M.; McBreen, J.; Grey, C. P. *Electrochem. Solid State Lett.* **2002**, *5*, A263.

some Ni metal displaced (or extruded) from $Li_2Ni_{0.5}Mn_{0.5}O_2$ (or $LiNi_{0.5}Mn_{0.5}O_2$). Both electrochemical processes are fairly reversible for this material and were observed to occur within a voltage window of approximately 1.25−1.0 V vs Li. It is worth noting that the performance of $Li/LiNi_{0.5}Mn_{0.5}O_2$ cells under moderate current rates (0.5−0.1 mA/cm^2) has shown 250−300 mA·h/g reversible capacity between 4.6 and 1.25 V.[39]

By understanding the electrochemical properties and structures of Ni−Mn mixed-metal layered oxides, we can begin to integrate the lithiated-layered structure Li_2MO_2 (M = metal ion) into new battery design concepts and technologies. Moreover, this new finding has implications for improving the electrochemical performance of lithium-ion cells because it may be possible to eliminate the first cycle capacity loss in graphite, alloy, or intermetallic Li-ion full cells by exploiting the Li_2MO_2 phase in a sacrificial first charge.

(39) Johnson, C. S.; Kim, J.-S.; Kropf, A. J.; Kahaian, A. J.; Vaughey, J. T.; Thackeray, M. M. *J. Power Sources*, in press.

Acknowledgment. We thank Dr. Lisa Utschig (ANL) for technical assistance in acquiring ICP-AES data. Support from the Office of Basic Energy Sciences, Division of Chemical Sciences, and the Office of Advanced Automotive Technologies, both of the U.S. Department of Energy, under Contract No. W-31-109-Eng-38 is gratefully acknowledged. Use of the Advanced Photon Source was supported by the U.S. Department of Energy, Office of Science, Office of Basic Energy Sciences, under Contract No. W-31-109-Eng-38. Work performed at MRCAT is supported in part by funding from the Department of Energy under Grant No. DEFG0200ER45811.

CM0204728